PERGAMON

International Journal of Heat and Mass Transfer 42 (1999) 2499–2508

International Journal of HEAT and MASS TRANSFER

Theoretical analysis of spreading and solidification of molten droplet during thermal spray deposition

H. Zhang

Department of Mechanical Engineering, State University of New York at Stony Brook, Stony Brook, NY 11794-2300, U.S.A.

Received 7 May 1998; in final form 9 November 1998

Abstract

A theoretical model for droplet spreading and solidification has been developed which accounts for simultaneous effects of surface tension, solidification and thermal contact resistance. Based on this model, an analytic solution for splat flattening ratio has been obtained as a function of Reynolds, Weber, Prandtl and Jakob numbers. Two different regimes, in terms of Reynolds and Weber numbers, have been identified where either the viscous dissipation or surface tension dominates. A map for splat flattening ratio has been generated for Reynolds number in the range of 10^4–10^6 and Weber number in the range of 5–5000. © 1999 Elsevier Science Ltd. All rights reserved.

Nomenclature

A constant
C constant
C_p specific heat [J kg^{-1} K^{-1}]
E_k kinetic energy [W m^{-3}]
E_p potential energy [W m^{-3}]
Ja Jakob number, $C_p(T_f-T_{si})/h_{fs}$
k thermal conductivity [W m^{-1} K^{-1}]
L_f work due to frictional forces [W m^{-3}]
m wetting coefficient
Pr Prandtl number, v_l/α_l
R droplet radius [m]
$R''_{t,c}$ contact resistance [m^2 K W^{-1}]
r radial coordinate [m]
Re Reynolds number, $2\rho w_0 R_0/\mu$
S parameter
s thickness of the deposited layer [m]
T temperature [K]
t time [s]
V volume [m^3]
w velocity [m s^{-1}]
We Weber number, $2\rho w_0^2 R_0/\sigma_l$
x axial coordinate [m].

Greek symbols
α thermal diffusivity [m^2 s^{-1}]
δ droplet thickness [m]
η liquid volume fraction
θ dimensionless temperature, $(T-T_{si})/(T_f-T_{si})$
λ constant
μ viscosity [kg s^{-1} m^{-1}]
ξ dimensionless spreading radius
ξ_m flattening ratio
ρ density [kg m^{-3}]
σ surface tension [N m^{-1}]
τ time at which solidification started [s]
ϕ_0 equilibrium contact angle [deg]
ω constant.

Subscripts
f fusion temperature
i interface
l melt
ls melt/solid
o initial
r radial coordinate
s deposited layer
si initial substrate temperature
sub substrate.

Superscripts
′ dimensional variable
¯ average variable.

1. Introduction

Thermal spray deposition processes begin with feed stock materials in powder form being injected into a

0017–9310/99/$ - see front matter © 1999 Elsevier Science Ltd. All rights reserved
PII: S0017–9310(98)00364–0

gas jet passing through a high temperature environment, where they are heated up, melted and accelerated towards a substrate where a thin deposited layer is formed after impingement, spreading and solidification. The spreading and solidification of the molten droplet involve rapid energy transport and microstructure formation. Due to the complex physical changes occurring in a very short time (less than 1 ms), it has been very difficult to develop a good understanding of the spray deposition processes and the associated physical phenomena [1–3].

During the last three decades, several theoretical studies have been carried out to analyze the deformation of the free surface and the evolution of the solidification front during the deposit formation [1, 4]. These models describe that a molten droplet when it impacts on a planar substrate, continuously deforms and solidifies. Most prevalent is the approach based on macroscopic mechanical energy balance, described mathematically as

$$\frac{\mathrm{d}}{\mathrm{d}t'}(E_\mathrm{k}+E_\mathrm{p}+L_\mathrm{f})=0 \tag{1}$$

where E_k, E_p and L_f are the kinetic energy, the potential energy and the work due to frictional forces, respectively, and t' is the time. Assuming that the droplet remains as a cylindrical disk during the deformation and the velocity distribution obeys

$$w_x=-Cx'^2, \quad w_\mathrm{r}=Cx'r' \tag{2}$$

Madejski [5, 6] developed a formula to calculate the splat flattening ratio, ξ_m, for different Reynolds number, Re and Weber number, We, as

$$\frac{3\xi_m^2}{We}+\frac{1}{Re}\left(\frac{\xi_m}{1.2941}\right)^5=1, \tag{3}$$

$$\text{for } We>100 \quad \text{and} \quad Re>100$$

in the absence of solidification. This model has been well supported by experiments [6–10]. If solidification is considered, the splat flattening ratio is obtained as

$$\xi_m=1.5344S^{-0.395}, \quad \text{for } Re\to\infty \quad \text{and} \quad We\to\infty \tag{4}$$

where S is a parameter obtained from the Neumann solution of the Stefan problem [7].

Modifications were made to Madejski's analysis [4, 8] to include the effect of adhesion tension through the equilibrium contact angle. Also, the solution of the Stefan problem by Carslaw and Jaeger [7] was incorporated into this analysis to represent the evolution of the solidification front and account for heat transfer among the molten droplet, deposited layer and substrate [1].

To preserve the mass conservation and retain the free surface shear stress free, Markworth and Saunders [9] proposed a higher-order velocity distribution as

$$w_x=\tfrac{2}{3}Ax'^2(x'-3\delta), \quad w_\mathrm{r}=Ax'r'(2\delta-x'), \tag{5}$$

where $A=3(\mathrm{d}R/\mathrm{d}t')/(2R\delta^2)$ is a function of time, R is the radius of the droplet, and δ is its thickness. Using the velocity distribution of equation (5) and following the Madejski's procedure, Delplanque and Rangel [11, 12] later developed an analytical solution to predict the splat flattening ratio as

$$\frac{3\xi_m^2}{We}+\frac{1}{Re}\left(\frac{\xi_m}{1.1626}\right)^5=1, \tag{6}$$

$$\text{for } We>670 \quad \text{and} \quad Re>140$$

without solidification. Similar to Madejski, these authors have also neglected the effect of wall adhesion. A numerical method was then used to solve the spreading problem together with solidification.

In this paper, a model for droplet spreading and solidification has been developed using the velocity distribution of equation (5) and accounting for the adhesion tension between the molten droplet and substrate. To examine the validity of the analytical solution, two-dimensional numerical models are used and compared with the analytical solutions. The effect of solidification rate that accounts for the thermal contact resistance on spreading has also been studied. A formula for splat flattening ratio has been proposed as a function of Reynolds, Weber, Prandtl and Jakob numbers. The model helps in identifying two deposit formation regimes, one in which the surface tension dominates and the other where viscous dissipation plays a dominant role.

2. Spreading and solidification

2.1. Effect of surface tension on droplet spreading

For a spherical droplet of initial radius R_0, impinging normally on a planar substrate, the kinetic energy can be obtained as

$$E_\mathrm{k}=2\pi\int_0^R r'\,\mathrm{d}r'\int_0^\delta \mathrm{d}x'\cdot\frac{1}{2}\rho(w_x^2+w_\mathrm{r}^2)$$

$$=\frac{3}{10}\pi\rho\left(\frac{\mathrm{d}R}{\mathrm{d}t'}\right)^2\delta R^2\left(1+\frac{11}{7}\frac{\delta^2}{R^2}\right). \tag{7}$$

where it is assumed that the droplet remains as a cylindrical disk during the deformation and the velocity distribution obeys equation (5). As suggested by Delplanque and Rangel [11], the work due to frictional forces can be calculated from

$$\frac{\mathrm{d}L_\mathrm{f}}{\mathrm{d}t'}=\frac{\pi R^2\mu}{\delta}\left(\frac{\mathrm{d}R}{\mathrm{d}t'}\right)^2\left(\frac{3}{2}+\frac{72}{5}\frac{\delta^2}{R^2}\right) \tag{8}$$

and the potential energy, that includes the surface tension forces acting on the melt–gas, solid–gas and melt–solid interfaces, can be written as

$$E_p = \sigma_l(\pi R^2 + 2\pi R\delta) + (\sigma_{ls} - \sigma_s)\pi R^2 = \sigma_l(1-m)\pi R^2 + \sigma_l 2\pi R\delta \quad (9)$$

where σ_l, σ_s, and σ_{ls}, are the surface tensions between the molten droplet and gas, the substrate and gas, and the molten droplet and substrate, respectively, and $m = \cos\phi_0$ is known as the degree of wetting or wetting coefficient, while $\sigma_s - \sigma_{ls}$ is often described as the wetting or adhesion tension [4, 8, 13]. Here, ϕ_0 is the equilibrium contact angle between the molten droplet and substrate. It should be noted that the cylindrical disk assumption requires that the dynamic contact angle be equal to 90°. During thermal spray deposition, the drop impact at high velocity (as high as 100 m s^{-1}) leads to a dynamic wetting condition at the spreading contact line [14]. Experiments have shown that the dynamic contact angle differs significantly from the equilibrium value [15, 16]. Therefore, the equilibrium contact angle can be different from 90°. In fact, the value is significantly different in thermal spray deposition.

Substituting equations (7)–(9) into equation (1), the energy balance equation can be written as

$$\frac{d}{dt'}\left[\frac{3}{10}\pi\rho\left(\frac{dR}{dt'}\right)^2\delta R^2\left(1+\frac{11}{7}\frac{\delta^2}{R^2}\right) + \sigma_l\pi R^2\left(1-m+\frac{2\delta}{R}\right)\right] + \frac{3}{2}\frac{\pi R^2\mu}{\delta}\left(\frac{dR}{dt'}\right)^2\left(1+\frac{48}{5}\frac{\delta^2}{R^2}\right) = 0. \quad (10)$$

Using the dimensionless variables,

$$\xi = R/R_0, \quad t = w_0 t'/R_0, \quad (11)$$

and Reynolds and Weber numbers as

$$Re = 2\rho w_0 R_0/\mu, \quad We = 2\rho w_0^2 R_0/\sigma_l, \quad (12)$$

equation (10) can be non-dimensionalized as

$$\frac{d}{dt}\left[\dot{\xi}^2\left(1+\frac{176}{63}\frac{1}{\xi^6}\right)\right] + \frac{5}{We}\frac{d}{dt}\left[\xi^2\left((1-m)+\frac{8}{3}\frac{1}{\xi^3}\right)\right] + \frac{45}{8}\frac{1}{Re}\xi^4\dot{\xi}^2\left(1+\frac{256}{15}\frac{1}{\xi^6}\right) = 0, \quad (13)$$

with the boundary conditions

$$\xi(0) = 1, \quad \dot{\xi}(0) = \sqrt{5/3}, \quad (14)$$

where $\pi\delta R^2 = 4/3\pi R_0^3$ has been used to satisfy the mass conservation. Different authors have used different values of $\dot{\xi}(0)$ [5, 11]. Here $\dot{\xi}(0)$ is taken as $\sqrt{5/3}$ since it provides a better agreement with the two-dimensional results.

Equation (13) can be solved numerically. To obtain a semi-analytic solution, the second, fourth, and sixth terms in equation (13) are neglected. The error introduced by the elimination of these terms depends on the value of ξ, and it is justified to say that the error will be small if $\xi > 3$. The spreading velocity of the droplet can then be derived as

$$\dot{\xi} = \sqrt{\frac{5}{3} - \frac{9}{16}\frac{\xi^5 - 1}{Re}}, \quad \text{for } We \to \infty \quad (15)$$

$$\dot{\xi} = \sqrt{\frac{5}{3} - \frac{5(1-m)(\xi^2-1)}{We}}, \quad \text{for } Re \to \infty \quad (16)$$

and the splat flattening ratio can be obtained as

$$\xi_m \approx 1.18Re^{1/5}, \quad \text{for } We \to \infty \quad (17)$$

$$\xi_m = \sqrt{\frac{We}{3(1-m)} + 1}, \quad \text{for } Re \to \infty \quad (18)$$

by setting $\dot{\xi} = 0$. An approximate estimate of ξ_m for other values of Reynolds and Weber numbers can be obtained from equation (13) as follows:

$$\frac{1}{Re}\left(\frac{\xi_m}{1.18}\right)^5 + \frac{3(1-m)(\xi_m^2 - 1.0)}{We} = 1.0. \quad (19)$$

The discrepancy between the analytical solution of equation (19) and the numerical solution of equation (13) is less than 5% for Re in the range of 10^4–10^6 and We in the range of 5–5×10^3. Equation (19) is very close to Madejski's solution, equation (3), if the wetting coefficient is taken as zero. The difference over Madejski's solution is due to the velocity profile of equation (5), and shows up in the coefficient of the first term, 1.18 instead of 1.29 in Madejski's model. A slightly different value, 1.16 instead of 1.18, has been obtained by Delplanque and Rangel [11]. The difference is due to the variation in initial conditions. Overall, the difference between the current model and Madejski's solution is minor for the case without adhesion tension.

To determine the deposit formation regimes in which either viscous dissipation or surface tension effect dominates, it is necessary to re-examine equation (19). The equation primarily constitutes of two terms:

$$Term\ I = \frac{1}{Re}\left(\frac{\xi_m}{1.18}\right)^5$$

and

$$Term\ II = \frac{3(1-m)(\xi_m^2 - 1.0)}{We}.$$

From the definition of Reynolds and Weber numbers, it is clear that *Term I* is proportional to viscosity, μ, and *Term II* to surface tension, σ. This indicates that *Terms I* and *II* represent the effects of viscous dissipation and surface tension, respectively. As the summation of these two terms equal unity, it is reasonable to assign $Term\ I = Term\ II = 0.5$, to identify the condition where viscosity dissipation and surface tension play equal roles in droplet spreading. Mathematically, this assignment leads to a relationship among Reynolds and Weber numbers and the wetting coefficient,

$$We = 6.33(1-m)Re^{0.4}. \quad (20)$$

It should be mentioned that a similar formulation was also proposed by Bennett and Poulikakos [4], that led to the criterion of

$$We = 2.80Re^{0.457}, \quad (21)$$

through the curve-fitting of numerical solutions. Apparently, equation (21) is valid only if the wetting coefficient is equal to zero.

By setting *Term I* > 0.9, the viscous dissipation dominant regime can be determined from

$$We > 40.0(1-m)Re^{0.4}. \quad (22)$$

Similarly, by setting *Term II* > 0.9, the surface tension dominant regime can be determined from

$$We < 1.85(1-m)Re^{0.4}. \quad (23)$$

The implication here is that when the criterion in equation (22) is satisfied, the surface tension effects can be neglected. Similarly, when equation (23) is valid, the viscous dissipation effects are negligible.

Since both Reynolds and Weber numbers are directly proportional to the initial diameter of the droplet, the spreading of a large droplet is controlled by the viscous dissipation effects, and the spreading of a small droplet is usually in the surface tension dominated regime. As a consequence, the experimental results obtained for large droplets may not be applicable to thermal spray deposition where molten droplets are much smaller, generally less than a few hundred microns.

2.2. Effect of solidification on droplet spreading

Solidification has been included in the Madejski's model through the mass loss from the molten state leading to an energy balance equation for spreading [5, 6]. Following a similar procedure, we can obtain the following equation by replacing δ by $\eta\delta$ in equation (10),

$$\frac{\mathrm{d}}{\mathrm{d}t'}\left[\frac{3}{10}\pi\rho\left(\frac{\mathrm{d}R}{\mathrm{d}t'}\right)^2\eta\delta R^2\left(1+\frac{11}{7}\frac{(\eta\delta)^2}{R^2}\right)+\sigma_1\pi R^2\left(1-m+\frac{2\eta\delta}{R}\right)\right] + \frac{3}{2}\frac{\pi R^2\mu}{\eta\delta}\left(\frac{\mathrm{d}R}{\mathrm{d}t'}\right)^2\left(1+\frac{48}{5}\frac{(\eta\delta)^2}{R^2}\right)=0. \quad (24)$$

where $\eta = 1 - V_s'/(4\pi R_0^3/3)$ is the liquid volume fraction, and $\delta = 4R_0/(3\xi^2)$ is the thickness of the droplet without solidification. According to Madejski, the volume of the solidified layer can be expressed as follows:

$$V_s' = \pi R_0^2\lambda'\sqrt{(\alpha_s t')} + \int_0^{t'} 2\pi R(\tau')\frac{\mathrm{d}R(\tau')}{\mathrm{d}\tau'}\lambda'\sqrt{[\alpha_s(t'-\tau')]}\,\mathrm{d}\tau' = \pi R^2\bar{s}', \quad (25)$$

where α_s is the thermal diffusivity of the deposited layer, λ' is a constant related to Jakob number, and $\bar{s}'$ is the average thickness of the deposited layer. Equation (24) can be non-dimensionalized as

$$\frac{\mathrm{d}}{\mathrm{d}t}\left[\eta\xi^2\left(1+\frac{176}{63}\frac{\eta^2}{\xi^6}\right)\right]+\frac{5}{We}\frac{\mathrm{d}}{\mathrm{d}t}\left[\xi^2\left((1-m)+\frac{8}{3}\frac{\eta}{\xi^3}\right)\right] + \frac{45}{8}\frac{1}{\eta Re}\xi^4\dot{\xi}^2\left(1+\frac{256}{15}\frac{\eta^2}{\xi^6}\right)=0 \quad (26)$$

where $\eta = 1-\bar{s}'\pi R^2/(4\pi R_0^3/3) = 1-\frac{3}{4}\xi^2\bar{s}$ and $\bar{s} = \bar{s}'/R_0$.

An accurate prediction of $\bar{s}$ depends on integration of equation (25) which requires a detailed two-dimensional simulation. If we assume that the deposited layer remains a circular conical shape, the volume of the deposited layer can be expressed as $0.5\pi(R_0^2+R^2)s'$, where s' is the thickness at the center. The average thickness, therefore, can be written as $\bar{s}' = (0.5+0.5/\xi^2)s'$. From two-dimensional simulations [17, 18], the shape of the deposited layer is somewhere between the cylindrical shape and the circular conical shape, which leads us to conclude that $0.5s' < \bar{s}' < s'$. Assuming $\bar{s}' = \omega s'$ and $\omega \approx 0.6-1.0$, a one-dimensional Stefan solution can be used to predict the dimensionless average thickness, $s = s'/R_0$ [7]:

$$\bar{s} = \omega s = \omega\lambda\sqrt{\alpha_s t/w_0 R_0} = \omega S\sqrt{t}, \quad (27)$$

where λ and S are constants related to the thermophysical properties of the molten droplet, deposited layer, and substrate [7]. Equation (26) can be solved using a numerical method. A semi-analytical solution can be generated by considering the individual contributions of the viscous, surface tension and solidification effects as follows

$$\frac{1}{Re}\left(\frac{\xi_m}{1.18}\right)^5+\frac{3(1-m)(\xi_m^2-1.0)}{We}+\omega S\left(\frac{\xi_m}{1.15}\right)^{2.5}=1.0. \quad (28)$$

The error is less than 8% between the numerical results of equation (26) and the analytical solutions of equation (28) for *Re* in the range of 10^4–10^6 and *We* in the range of $5-5\times10^3$. It is evident from equation (28) that the splat flattening ratio decreases as the solidification rate increases.

2.3. Effect of contact resistance on thermal spray deposition

Microstructures of the deposit depend on the solidification rate and heat flux direction of many individual molten droplets. Droplet spreading and solidification are therefore key to microstructures and properties of the deposit. Phase content, grain size, degree of solute supersaturation, interlamellar bond strength, thermal conductivity and many other features of the deposit are intimately affected by the spreading and solidification. To

introduce contact resistance, consider two semi-infinite solids of different materials with uniform temperatures T_m and T_{sub}, brought together at time $t = 0$. In this case, the interface temperature T_i will be a constant, given by [19]

$$T_i = \frac{k_l T_l/\sqrt{\alpha_l} + k_{sub} T_{sub}/\sqrt{\alpha_{sub}}}{k_l/\sqrt{\alpha_l} + k_{sub}/\sqrt{\alpha_{sub}}} \tag{29}$$

The substrate can be considered as a semi-infinite solid, whereas the droplet can be considered as a semi-infinite solid only at the beginning of the contact. If the contact interface temperature is lower than the nucleation temperature (undercooling level can be more than 400 K during the thermal spray deposition), the solidification will start. If the interface temperature is larger than the nucleation temperature, it will remain unchanged until the temperature boundary layer reaches to the top surface of the molten droplet whose thickness is decreased with time. The contact surface temperature will then decrease, and the solidification will start as soon as it reaches the nucleation temperature. Almost all of the theoretical studies reported in the literature assume that the solidification starts immediately after the molten droplet touches the substrate. At this current stage, we will use the same assumption and will not consider the non-equilibrium effects on solidification, and write the solidification interface velocity in two-dimensional form as

$$\frac{ds}{dt} = \frac{Ja}{RePr}\left[1 + \left(\frac{\partial s}{\partial r}\right)^2\right]\left[\frac{k_s}{k_l}\frac{\partial \theta_s}{\partial x} - \frac{\partial \theta_l}{\partial x}\right], \tag{30}$$

where $Pr = \nu_l/\alpha_l$ is the Prandtl number, and $Ja = C_p(T_f - T_{si})/h_{fs}$ is the Jakob number. Here, the dimensionless temperature, θ is defined as $(T - T_{si})/(T_f - T_{si})$, and the densities and specific heats of the solid and liquid phases are assumed to be equal. If the curvature effect is neglected or $(\partial s/\partial r)^2 \ll 1$, the interface velocity can be expressed in one-dimensional form. Further assume that (a) the heat loss through the molten droplet can be neglected and the temperature at the solidification interface remains at the fusion temperature, (b) the temperature at the substrate surface remains constant at the substrate temperature, (c) the temperature profile is linear in the deposited layer (Ja is small) [19], and (d) the molten droplet has a perfect contact with the substrate ($R''_{t,c} = 0$). Equation (30) can then be simplified as

$$\frac{ds}{dt} = \frac{Ja}{RePr}\frac{k_s}{k_l}\frac{1}{s} \tag{31}$$

which has a straight-forward solution as

$$s = \sqrt{2t\left(\frac{Ja}{RePr}\frac{k_s}{k_l}\right)} = S\sqrt{t} \tag{32}$$

where $S = \sqrt{(2Ja/RePr)(k_s/k_l)}$.

However, the assumption (b) is not applicable in many applications. For example, is heat conduction in the substrate is appreciable, the temperature distribution in the substrate must be considered through an error function solution that will modify equation (31) to yield [19],

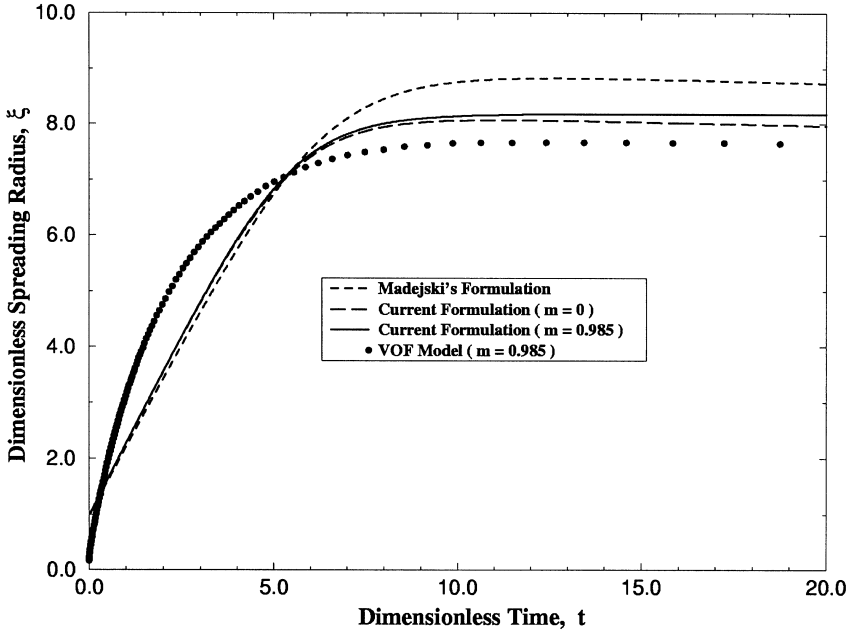

Fig. 1. The dimensionless spreading radius predicted by the two-dimensional model compared with the analytical solutions for $Re = 1.6 \times 10^4$, $We = 4.0 \times 10^3$, and the wetting coefficient of $m = 0.985$.

$$\frac{ds}{dt} = \frac{Ja}{RePr}\frac{k_s}{k_l}\left(\frac{1}{s+\sqrt{(2\pi t/RePr)(\alpha_{sub}/\alpha_l)}(k_s/k_{sub})}\right). \quad (33)$$

Similarly, if the thermal contact resistance, $R''_{t,c}$, between the droplet and the substrate is important, equation (31) can be modified to yield

$$\frac{ds}{dt} = \frac{Ja}{RePr}\frac{k_s}{k_l}\frac{1}{s+(k_s R''_{t,c}/R_0)}. \quad (34)$$

The interface position is then taken as

$$s = -(k_s R''_{t,c}/R_0)+\sqrt{(k_s R''_{t,c}/R_0)^2+S^2 t} \quad (35)$$

and the solidification rate,

$$\frac{ds}{dt} = (S^2/2)/\sqrt{(k_s R''_{t,c}/R_0)^2+S^2 t}. \quad (36)$$

It is evident that the solidification rate is reduced when the thermal contact resistance is included. However, the thermal contact resistance is important at the beginning of the solidification process. As time increases, the effect of thermal conductivity becomes important and the flattening ratio will be less affected by the contact resistance. As a result, equation (28), may remain valid for most of the solidification process.

3. Results and discussion

To examine the accuracy of the current model, the present results have been compared with Madejski's solution as well as that obtained by numerical computations. To perform the numerical simulations of coupled spreading and solidification processes, a two-dimensional model has been developed that uses SOLA-VOF [17, 20, 21] as a fluid solver for the deformation of free surface and a local 1D solution ($S\sqrt{t-\tau}$) where the solid front advances in the direction normal to the solid/liquid interface [10]. Figure 1 shows the dimensionless spreading radius predicted for $Re = 1.6\times10^4$, $We = 4.0\times10^3$ and $m = 0.985$ (equilibrium contact angle is equal to 10°) without solidification. The parameters used in Fig. 1 correspond to the impingement of a nickel droplet of 100 μm diameter with an impacting velocity of 100 m s^{-1}. A small discrepancy between the current model and the two-dimensional result is observed in the predictions of splat flattening ratio.

The evolutions of the free surface and temperature distributions during spreading and solidification are shown in Fig. 2. Two-dimensional results demonstrate that the droplet forms a thin film sheet spreading radially at a high speed. The maximum velocity of the radial wall sheet jet at the earlier stages of impingement in Fig. 1 is about three times that of the initial impact velocity, which agrees with the results of Trapaga and Szekely [17]. The spreading rates predicted by the analytical model are, however, much lower than that obtained from the two-dimensional simulations and experiments. It is evident that the analytical solutions fail to correctly predict the

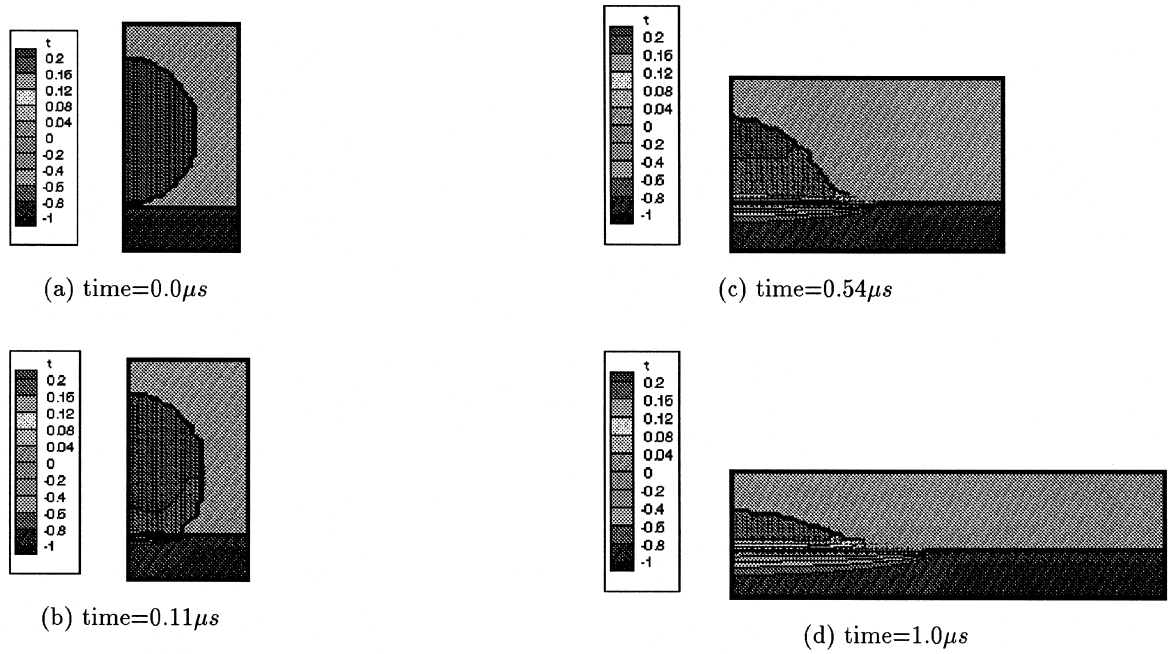

Fig. 2. Free surface evolution and temperature distribution of a 100 μm diameter nickel droplet impinging at a velocity of 100 m s^{-1}. Two-dimensional numerical solution using 162×62 non-uniform grids ($Re = 1.6\times10^4$, $We = 4.0\times10^3$, $m = 0$, $Pr = 0.01$, and $S = 0.001$).

spreading rate of the wall sheet jet. The under-prediction of the wall sheet jet velocity is due to the unrealistic assumption of the cylindrical disk shape during the deformation. Although it may be possible to develop an improved model based on the shape deformation from a spherical to a cylindrical disk, that has not been considered either by the present work nor by others. They have focused only on the effects of the surface tension and solidification on the splat flattening ratio.

A number of experimental studies [3, 22] has shown that the substrate temperature plays an important role in determining whether the plasma sprayed droplets retain their coherence and spread out in the form of ideal disks or splatter into several interconnected fragments. This

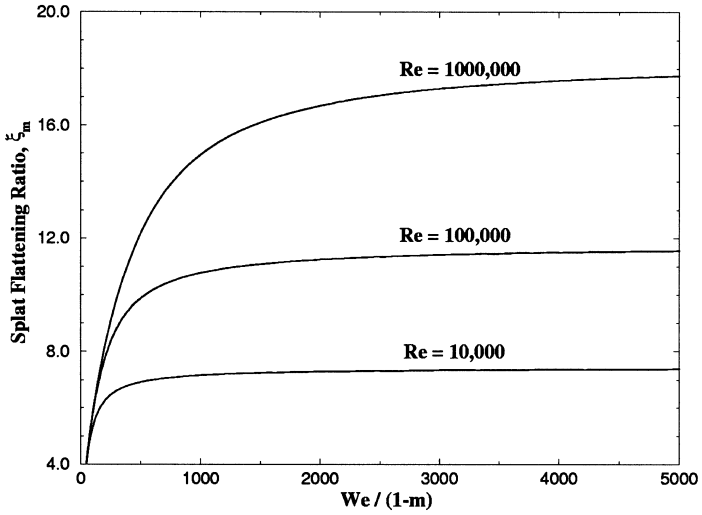

Fig. 3. Map of the splat flattening ratio in the range of $Re = 10^4 - 10^6$ and $We/(1-m) = 5-5000$.

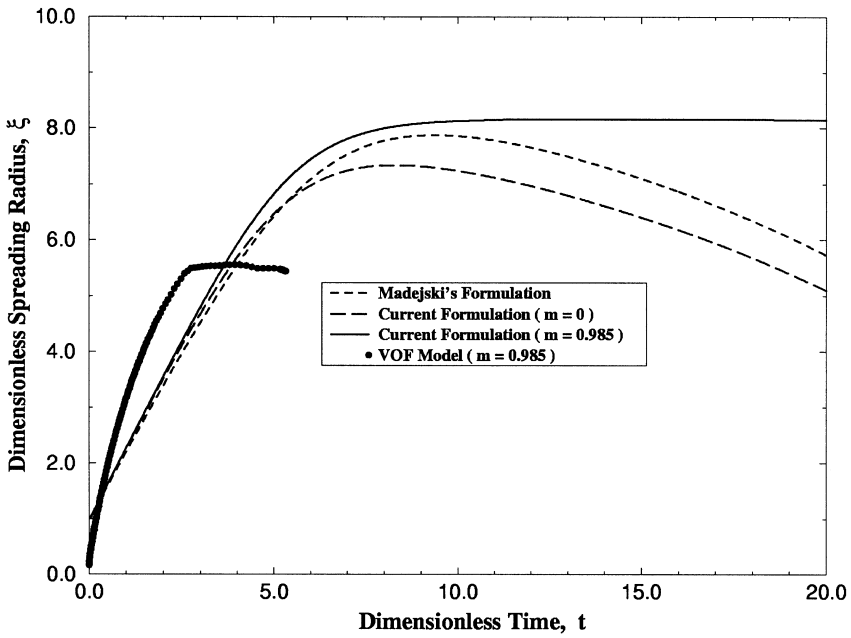

Fig. 4. The dimensionless spreading radius predicted by various models for $Re = 1.6 \times 10^4$, $We = 3.0 \times 10^2$, and the wetting coefficient of $m = 0.985$.

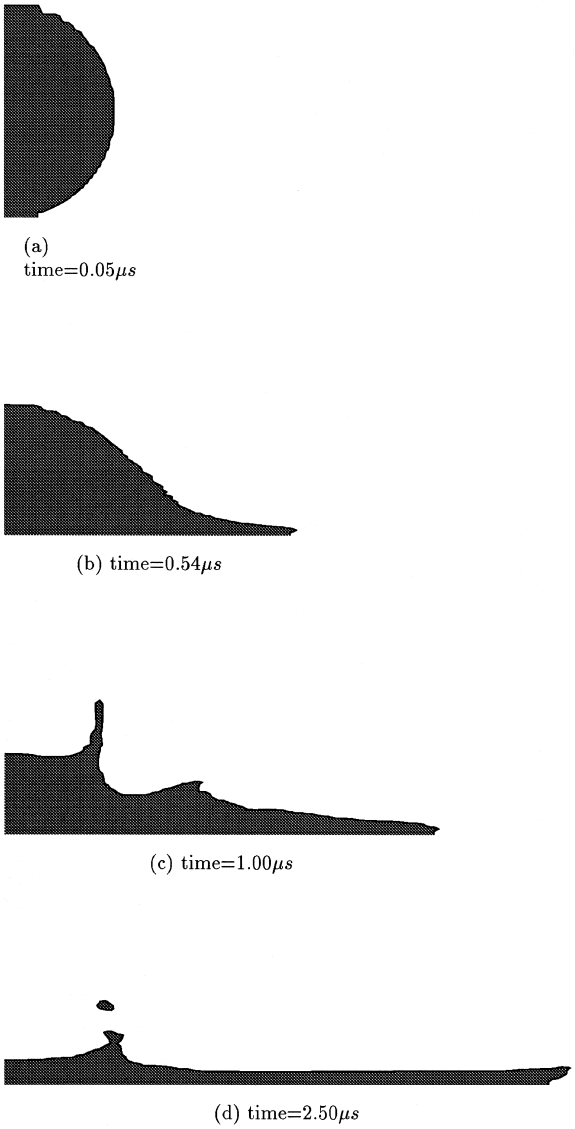

Fig. 5. Free surface break-up during the spreading, for $Re = 1.6 \times 10^4$, $We = 1.0 \times 10^3$, and the wetting coefficient of $m = 0$.

phenomenon has been attributed to some physico-chemical changes which occur when the substrate temperature is higher than the so-called 'transition temperature' [3] and allows the liquid to 'wet' the substrate, spread evenly and adhere well on the substrate. The model developed here assumes an ideal disk shape, and, therefore, cannot be used to predict the splash phenomenon. However, it can consider the 'wettability' through the wetting coefficient.

A splat flattening ratio map for various applications is shown in Fig. 3 which has been obtained by solving equation (10). Equation (19) has been used to examine the results. The difference between the predictions by equation (10) and equation (19) is less than 5% in the range of Re and We considered in Fig. 3. Information on accurate values of the wetting coefficient at different substrate temperatures is therefore important because it controls the droplet spreading. In the case of small Weber number, the flattening ratio obtained from the two-dimensional simulations is smaller than that predicted analytically, as shown in Fig. 4. As the Weber number decreases, a wavy pattern develops on the free surface due to Rayleigh instability. This feature has not been included in any analytical model. A wavy free surface has been observed in the case of $We = 300$, $Re = 1.6 \times 10^4$, and the wetting coefficient of 0.985. In addition to wavyness, the free surface may also break. Figures 5 and 6 show the free surface deformation and the droplet detach-

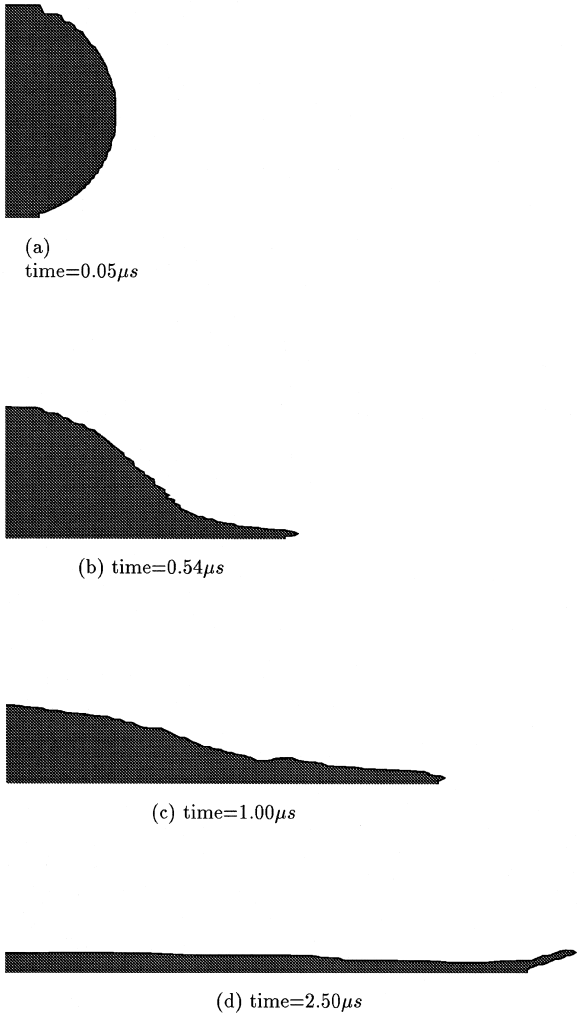

Fig. 6. Droplet detachment at the end of the process, for $Re = 1.6 \times 10^4$, $We = 1.0 \times 10^3$, and the wetting coefficient of $m = 0.985$.

ment at the outer edge during the impingement, for $Re = 1.6 \times 10^4$ and $We = 1.0 \times 10^3$ with two different wetting coefficients of 0 and 0.985 (without solidification), respectively. The analytical solution reveals that $We/(1-m)$ is an important parameter in determining the splat flattening ratio. The wetting coefficient changing from 0 to 0.985 results in the value of $We/(1-m)$ changing from 1.0×10^3 to 6.58×10^4, further demonstrating the importance of the wetting coefficient.

The above discussions are limited to forward spreading. Experimental observations indicate that the droplet can not only expand, but can also contract after it reaches its maximum lateral position. The backward movement can, sometimes, lead to the droplet bouncing off the substrate [14]. Figure 7 shows the effects of backward wetting coefficient and solidification rate on the deposition thickness. In Fig. 7, the splat flattening ratio decreases as the solidification rate increases. For the backward wetting coefficient of 0.985, the backward velocity is very small, and the droplet remains at the maximum spreading position. Solidification takes place under almost stationary droplet conditions. On the other hand, the result of $m = 0.82$ shows that the backward movement is much faster than that of $m = 0.985$. For a high solidification rate of $S = 0.005$, the droplet is able to solidify before it moves back to the spherical shape. For a low solidification rate of $S = 0.001$, the backward velocity is faster than the solidification rate, and the droplet may bounce off the substrate. These simulations clearly indicate the importance of the solidification rate and backward wetting coefficient.

4. Conclusion

An improved model has been developed that accounts for the surface tension effects at the melt–gas, solid–gas and solid–melt interfaces, as well as solidification. An

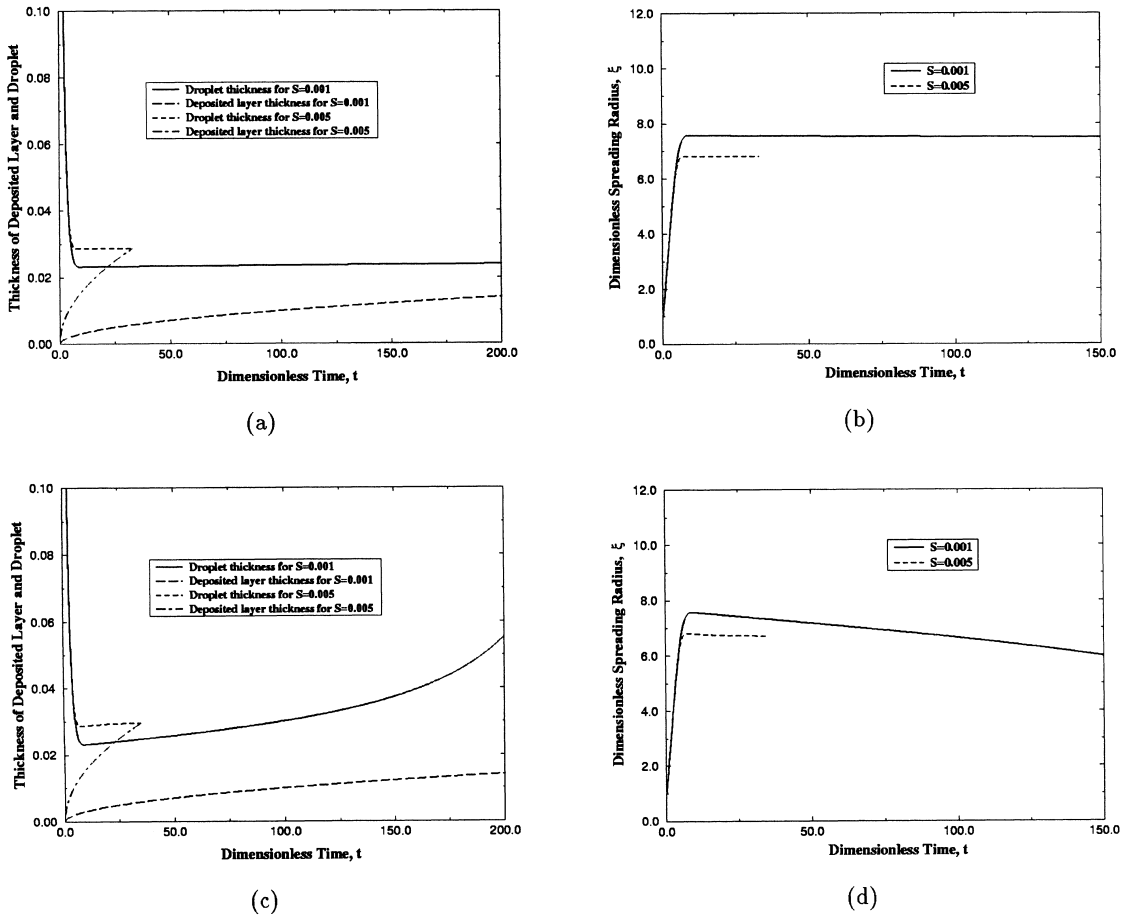

Fig. 7. Thickness of the deposited layer (bottom curve) and the droplet (upper curve) and dimensionless spreading radius for $Re = 1.6 \times 10^4$, $We = 1.0 \times 10^3$, $\omega = 1$ with the forward wetting coefficient of zero, and the backward wetting coefficient of 0.985 (a, b) and 0.82 (c, d).

analytic solution for the splat flattening ratio has been obtained as follows:

$$\frac{1}{Re}\left(\frac{\xi_m}{1.18}\right)^5+\frac{3(1-m)(\xi_m^2-1.0)}{We}+\omega S\left(\frac{\xi_m}{1.15}\right)^{2.5}=1.0. \tag{37}$$

The deposition thickness is estimated by

$$s=-(k_s R''_{t,c}/R_0)+\sqrt{(k_s R''_{t,c}/R_0)^2+S^2 t}. \tag{38}$$

The model reveals that the thermal contact resistance delays solidification and decreases the solidification rate.

A map of the splat flattening ratio has been generated for Re in the range of 10^4–10^6 and $We/(1-m)$ in the range of 5–5×10^3. Two regimes, in terms of Reynolds and Weber numbers, have been identified where either the viscous dissipation or surface tension dominates.

$We < 1.85(1-m)Re^{0.4}$,

surface tension dominant regime

$We > 40.0(1-m)Re^{0.4}$,

viscous dissipation dominant regime.

The numerical studies show that both the backward wetting coefficient and solidification rate play important roles in determining the splat flattening ratio and deposition thickness. The possibility that the droplet can bounce off the substrate is increased as the backward wetting coefficient decreases and the solidification rate decreases.

Acknowledgements

This research was supported by NSF grant no. CTS-9711135 and NSF MRSEC Center for Thermal Spray Research under the award no. DMR 9632570.

References

[1] R.C. Dykhuizen, Review of impact and solidification of molten thermal spray droplets, Journal of Thermal Spray Technology 3 (4) (1994) 351–361.
[2] D. Poulikakos, J.M. Waldvogel, Heat transfer and fluid dynamics in the process of spray deposition, Advances in Heat Transfer 28 (1996) 1–74.
[3] A. Vardelle, N.J. Themelis, B. Dussoubs, M. Vardelle, P. Fauchais, Transport and chemical rate phenomena in plasma sprays, Journal of High Temperature Processes 1 (1997) 295–314.
[4] T. Bennett, D. Poulikakos, Splat-quench solidification: estimating the maximum spreading of a droplet impacting a solid surface, Journal of Materials Science 28 (1993) 963–970.
[5] J. Madejski, Solidification of droplets on a cold surface, International Journal of Heat and Mass Transfer 19 (1976) 1009–1013.
[6] J. Madejski, Droplets on impact with a solid surface, International Journal of Heat and Mass Transfer 26 (1983) 1095–1098.
[7] H.S. Carslaw, J.C. Jaeger, Conduction of Heat in Solids, Clarendon Press, Oxford, 1984.
[8] E.W. Collings, A.J. Markworth, J.K. McCoy, J.H. Saunders, Splat-quench solidification of freely falling liquid-metal drops by impact on a planar substrate, Journal of Materials Science, 25 (1990) 3677–3682.
[9] A.J. Markworth, J.H. Saunders, An improved velocity field for the Madejski splat-quench solidification model, International Journal of Heat and Mass Transfer 35 (1992) 1836–1837.
[10] R.H. Delplanque, E.J. Lavernia, R.H. Rangel, Multidimensional solidification model for the description of micro-pore formation in spray deposition processes, Proceedings of the ASME Heat Transfer Division, IMECE HTD-Vol. 317-2, ASME, New York 1995, pp. 511–521.
[11] J.-P. Delplanque, R.H. Rangel, An improved model for droplet solidification on a flat surface, Journal of Materials Science 32 (1997) 1519–1530.
[12] X. Bian, J.-P. Delplanque, R.H. Rangel, Droplet deposition: comparison of models, numerical simulation and experimental results, Proceedings of the 32nd National Heat Transfer Conference, HTD-Vol. 347, ASME, New York, 1997, pp. 75–82.
[13] G.S.H. Lock, Latent Heat Transfer: An Introduction to Fundamentals, Oxford University Press, Oxford, UK, 1994, pp. 27–50.
[14] R. Bhola, S. Chandra, Splat solidification of tin droplets, Proceedings of the 9th International Thermal Spray Conference, ASM International, Materials Park, OH, 1996, pp. 657–663.
[15] V.E.B. Dussan, S.H. Davis, On the motion of a fluid–fluid interface along a solid surface, Journal of Fluid Mechanics 65 (1974) 71–91.
[16] V.E.B. Dussan, On the spreading of liquids on solid surfaces: static and dynamic contact lines, Annual Review of Fluid Mechanics 11 (1979) 371–400.
[17] G. Trapaga, J. Szekely, Mathematical modeling of the isothermal impingement of liquid droplets in spraying processes, Metallurgical Transactions 22B (1991) 901–914.
[18] G. Trapaga, E.F. Matthys, J.J. Valencia, J. Szekely, Fluid flow, heat transfer, and solidification of molten metal droplets impinging on substrates: comparison of numerical and experimental results, Metallurgical Transactions 23B (1992) 701–718.
[19] A.F. Mills, Heat Transfer, IRWIN, Boston, MA, 1992, pp. 147–192.
[20] B.D. Nichols, C.W. Hirt, R.S. Hotchkiss, SOLA-VOF: A Solution Algorithm for Transient Fluid Flow with Multiple Free Boundaries, Los Alamos, NM, LA-8355, 1980.
[21] H. Liu, E.J. Lavernia, R.H. Rangel, Numerical simulation of substrate impact and freezing of droplets in plasma spray processes, Journal of Physics D: Applied Physics 26 (1993) 1900–1908.
[22] M. Fukumoto, S. Katoh, I. Okane, Splat behavior of plasma sprayed particles on a flat substrate surface, Proceedings of International Thermal Spray Conference, ASM International, Materials Park, OH, 1995, pp. 353–358.